

Effect of auxiliary TIG arc on formation and microstructures of aluminum alloy/stainless steel joints made by MIG welding–brazing process

Hong-tao ZHANG, Ji-hou LIU, Ji-cai FENG

Shandong Provincial Key Laboratory of Special Welding Technology, School of Materials Science and Engineering, Harbin Institute of Technology at Weihai, Weihai 264209, China

Received 12 September 2013; accepted 20 January 2014

Abstract: A new hybrid welding process was successfully used to join aluminum alloy and stainless steel. In the MIG welding–brazing process, the lower thermal conductivity of steel can cause dramatic change of temperature gradient on steel surface, while the auxiliary TIG arc can change this phenomenon by heating the steel side. The auxiliary TIG improved the wettability of molten metal, resulting in the molten metal spreading fully on upper surfaces, front and back surface of steel, forming a sound brazing joint; the content of Cr and Ni elements in IMCs layer was increased, which can enhance the quality of the layer; and the microstructure of IMCs layer also was improved, increasing the bonding strength with the weld seam. The average tensile strength of the joint obtained with auxiliary TIG arc (146.7 MPa) was higher than that without auxiliary TIG arc (96.7 MPa).

Key words: welding–brazing; auxiliary TIG arc; wettability; intermetallics layer; mechanical property

1 Introduction

Joining of dissimilar metals provides not only the structure welded with the characteristics of dissimilar materials, including physical, chemical, and mechanical properties, but also a way of reducing the mass of the structure and its energy consumption [1–3]. Thus, joining aluminum alloy to stainless steel is a topic that has received much attention in recent years. However, this process is challenging because of the large differences between aluminum alloy and stainless steel in terms of thermo-physical properties, such as melting point, and near-zero solid solubility of iron in aluminum [4–6]. In particular, a strong tendency for brittle Fe–Al intermetallic compounds (IMCs) to form at elevated temperatures during the fusion-welding process should be considered [7]. The large thermo-physical differences in melting point, thermal conductivity, and thermal expansion coefficient can lead to high residual stress in the resultant welds after fusion welding. The welding structure may suffer from heavy cracking in service due to brittleness [8].

Many welding methods have been used in the attempt to achieve the reliable joining of aluminum and

steel, including solid-state and fusion-welding [9–14]. In the above mentioned processes, the geometry and dimensions of the workpieces are often limited, and some of the methods need high pressure, high energy, and long working time, all of which imply high production cost and low production efficiency. Recently, new focus has been placed on welding–brazing processes [15–18], for their high productivity. In previous studies, the focal point was on controlling the excessive formation of IMCs to reduce joint brittleness.

In this study, a new hybrid welding process is successfully formulated to improve the microstructure and mechanical properties of aluminum and stainless steel hybrid joints. In the MIG welding–brazing process, a synchronous TIG arc is used to heat the steel. A higher-temperature field is established on the steel side to promote the spreadability of the liquid filler metal. The surface appearances of the welds and the interfacial microstructure of the joints with or without the synchronous TIG arc are contrastively analyzed by optical micrograph (OM), scanning electron microscopy (SEM), energy dispersive spectrometry (EDS), and X-ray diffraction (XRD). The results show that the auxiliary TIG arc provides a new way to improve joints obtained from dissimilar metals.

2 Experimental

2.1 Materials and filler metals

The base metals were 7005 aluminum alloy and stainless steel (321) plates of 3.5 mm in thickness. 1.2-mm diameter 1100 pure aluminum welding wire was adapted as filler metal. The chemical compositions of base material and filler metal are listed in Table 1.

Table 1 Chemical composition of base metals and filler metal (mass fraction, %)

Metal	Zn	Fe	Mn	Ni	Cr	Al
7005	4.0–5.0	0.35	0.2–0.7	–	0.3	Bal.
321	–	Bal.	2.0	8–11	17–19	–
1100	0.05	0.10	–	–	–	Bal.

2.2 MIG welding–brazing process with auxiliary TIG arc

The dimensions of all materials plates were 80 mm×150 mm×3.5 mm, and the single-V groove was opened in the joint, with a bevel angle of 40° in steel side and 30° in aluminum side. The oxide film at the welding location was cleaned with sandpaper and acetone before experiment. The flux suspension (KAlF₄ and K₃AlF₆ eutectic), in which the flux powder was dissolved in organic solvent, was applied to the front surface of the steel with 0.2–0.5 mm in thickness and 10 mm in width homogeneously. The schematic diagram of the joining process is shown in Fig. 1.

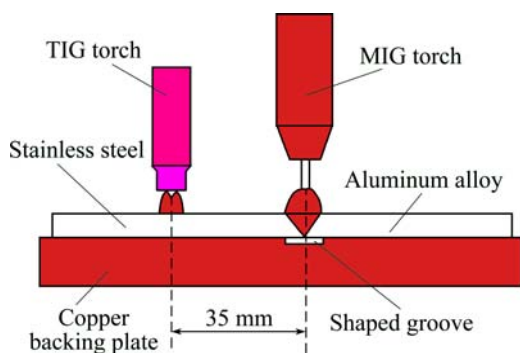


Fig. 1 Schematic diagram of hybrid welding process

As shown in Fig. 1, the auxiliary TIG torch was attached to parallel position side of the main MIG torch by a special fixture. The TIG torch was placed over the steel side; the distance between the centers of two torches was controlled in 35 mm; the two torches were controlled by two welding power sources respectively and the TIG torch and the MIG torch were moved synchronously during welding process. In order to reflect the effect of the auxiliary TIG arc, two contrast experiments were carried out, with or without the

auxiliary TIG arc. Two sets of welding parameters are listed in Table 2. Three dissimilar metal joints were made by per set.

Table 2 Welding parameters for joining aluminum alloy to stainless steel

No.	Welding current/A	Welding voltage/V	Welding speed/(cm·min ⁻¹)	TIG current/A
1	135	23	40	–
2	135	23	40	60

2.3 Analysis methods

After welding, metallographic specimens of typical cross-section of the welds were cut and then the specimens were polished by a series of metallographic sandpapers of SiC grades. The Keller's reagent was used to etch the metallographic specimens to reveal the general microstructure of the joints. The macro-feature of the joints was analyzed by OM and the joint microstructures and chemical compositions of typical phases were analyzed by scanning electron microscopy (SEM) with energy dispersive spectrometer (EDS). The phase composition of interfacial layer between fusion zone and solid steel was examined by X-ray diffraction. Six specimens with 10 mm in width cut perpendicular to the weld were used to evaluate the tensile property of the joint with a loading rate of 1 mm/min. The hardness distribution of the joints was also analyzed with a Vicker micro-hardness tester under 10 N loading force for 10 s holding time.

3 Results and discussion

3.1 Surface appearance and macrostructure

Figure 2 shows the surface appearance of the butt joints of aluminum alloy and stainless steel obtained by welding–brazing process. Figure 2(a) shows the surface appearance of No. 1 joint which was obtained by MIG welding–brazing process without TIG arc. Figure 2(b) shows the surface appearance of No. 2 joint which was obtained by MIG welding–brazing process with an auxiliary TIG arc. There are no obvious welding defects, such as crack, undercutting or incomplete fusion in the welded seam. There is residual flux on the steel surface near the welded seam, but the amount of residual flux on the No. 2 joint is less than that on the No. 1 joint. The auxiliary TIG arc makes the upper surface of steel have higher temperature, which can accelerate the evaporation of flux. The edge of No. 2 joint is more flat than that of No. 1 joint and the width of the seam of No. 2 joint is also little wider than that of No. 1 joint. The previous result shows that the auxiliary TIG arc brings additional heat to promote the spreading width of the molten metal.



Fig. 2 Appearances of welding-brazing joint: (a) No. 1 joint; (b) No. 2 joint

The typical cross-sections of the dissimilar metals butt joints obtained by MIG welding–brazing process is shown in Fig. 3. Both joints have typical feature of the MIG welding–brazing joint: on aluminum side, the low-melting aluminum base metal and the molten filler metal form the welding joint under the arc action; in contrasts, on steel side, the arc cannot make the steel surface melt, which has a high melting point, the molten metal spreads on the surface of steel to form a brazing joint.

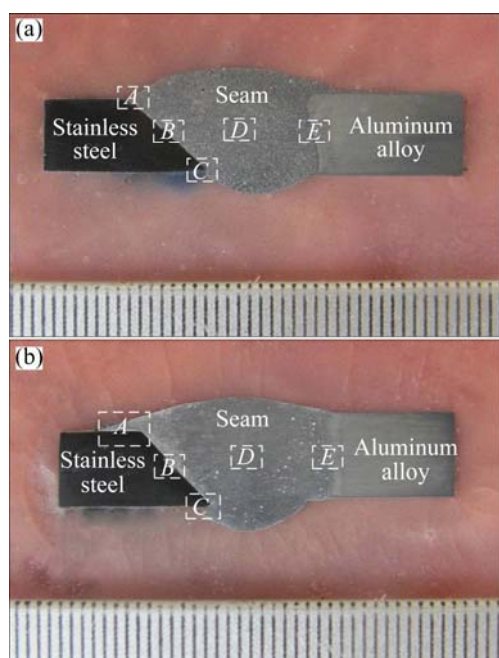


Fig. 3 Cross-sections of butt joint of aluminum to steel: (a) No. 1 joint; (b) No. 2 joint

The obvious difference between two sets of joints exist in the molten metal spreading behaviour as denoted by zone *A* and zone *C* in Fig. 3. When joining aluminum to steel with an auxiliary TIG arc, the molten metal spreads more fully on upper surface, groove surface and back surface than on that made without TIG arc, as shown in Fig. 4.

It is well known that the thermal conductivity of aluminum alloy is higher than that of steel, which can make the temperature gradient on steel surface greater than on aluminum alloy surface in welding process, while the auxiliary TIG arc can change this phenomenon by heating the steel side. The slight change of temperature gradient on steel surface can make the spreading process of molten metal on steel surface smoother, forming a sound brazing joint.

3.2 Microstructures of joints

Figure 5 shows the SEM images of zone *B* in Figs. 3(a) and (b). The average thickness of IMCs layers of No. 1 and No. 2 joints is less than the limited value of 10 μm [19] as shown in Figs. 5(a) and (b). The IMCs layer of No. 1 joint near steel side presents a serrated shape and some lath-shaped intermetallic compound grows into the seam. At the same time, some massive intermetallic compounds distribute in the seam near steel side. The thickness of IMCs layer of No. 2 joint is relatively homogeneous and there is no abnormal growth of lath-shaped intermetallic compound near steel side. The IMCs layer of No. 2 joint in steel side presents a jagged line, and it presents a needle-like crystal oriented toward the seam. This structure can cause a “pinning effect” between the layer and seam, enhancing the property of brazing joint, as shown in Fig. 5(b).

The phase chemical compositions of points *A*, *B*, *C* and *D* in Fig. 5 analyzed by EDS analysis method are shown in Table 3. The content of Al atom in layer from steel side to seam side increased from 74.26% to 81.63%, while Fe atom decreased from 17.53% to 10.19%, in the composition of points *A* and *B*. This change of Al and Fe was adapted to the composition of points *C* and *D*: Al increased from 70.68% to 80.12% and Fe atom decreased from 18.65% to 9.59%. This means that there are two different phase structures of IMCs layer near steel side and aluminum side, respectively. According to the Al–Fe binary phase diagram [20] and some researches about the IMC layer in Al–Fe welding–brazing process [21,22], the interfacial IMCs layer mainly consists of Fe_2Al_5 and FeAl_3 phases.

The contents of Cr and Ni at points *C* and *D* in No. 2 joint are higher than those at points *A* and *D*, especially the content of Ni. The auxiliary TIG arc makes the surface of steel have higher temperature, improving the diffusion of Cr and Ni from steel substrate to IMCs layer,

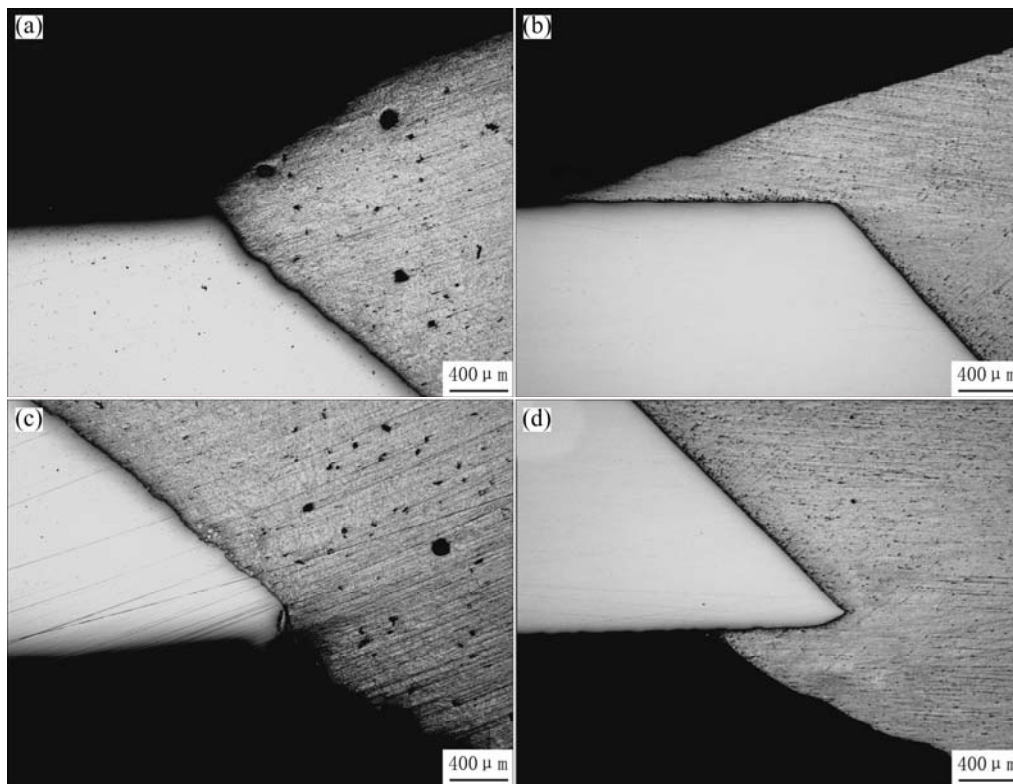


Fig. 4 Spreading characteristics of molten metal on surface of steel: (a) Upper surface of No. 1 joint (zone *A* of Fig. 3(a)); (b) Upper surface of No. 2 joint (zone *A* of Fig. 3(b)); (c) Back face of No. 1 joint (zone *C* of Fig. 3(a)); (d) Back face of No. 2 joint (zone *C* of Fig. 3(b))

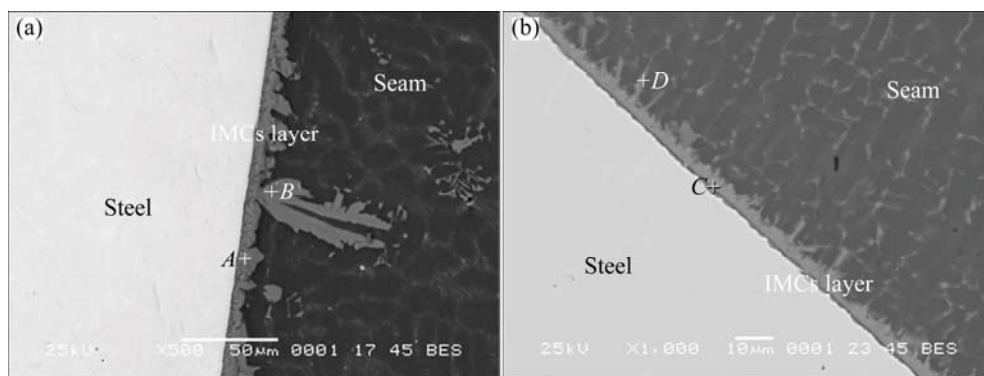


Fig. 5 SEM images in IMCs layer of butt joint: (a) Zone *B* in Fig. 3(a); (b) Zone *B* in Fig. 3(b)

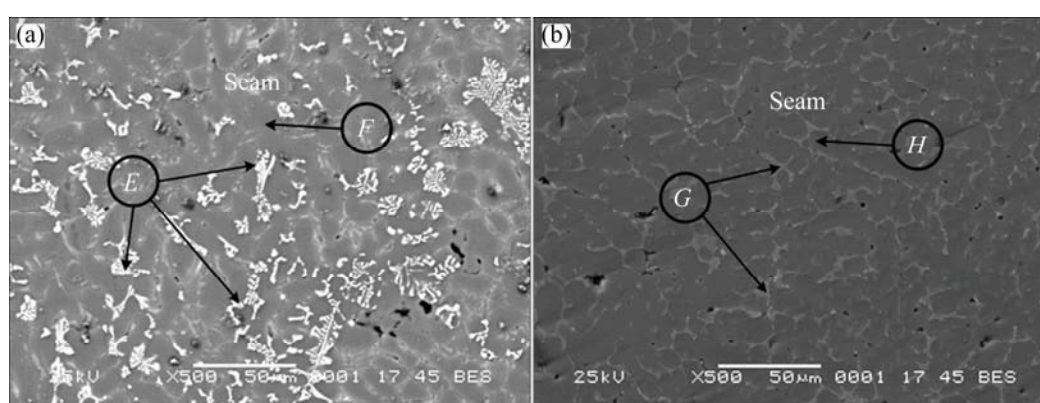
and the dissolved Cr and Ni substituting Fe in IMCs layer can enhance the quality of the layer [23].

Figure 6 shows the SEM backscattering images of seam center zone *D* in Figs. 3(a) and (b) and EDS analysis results in Table 3 were also used to depict the microstructure characteristics. The white undissolved phases, as shown in Fig. 6(a), were analyzed to give composition of 4.56% Fe, 1.43%Mg, 3.18%Zn and balance Al. The phases are thought to consist of Al–Fe and Mg–Zn compounds. Though the white undissolved phases are not present in the seam of No. 2 joint, as shown in Fig. 6(b), the result of the EDS analysis of point *G* at grain boundary shows that the diffused

elements were well dissolved at the grain boundary, without the formation of white phases. Comparing the content of element in $\alpha(\text{Al})$ matrix of two joints by the EDS analysis of points *F* and *H*, the contents of elements in $\alpha(\text{Al})$ matrix of No. 1 joint were so little without the presence of Cr and Ni, but the contents of elements in $\alpha(\text{Al})$ matrix of No. 2 joint were a little higher than those of No. 1, especially the contents of Cr, Ni, and Fe. In the seam center of No. 2 joint the dissolved Fe atoms diffuse uniformly in the molten metal for the additional heating effect of auxiliary TIG arc and then mainly enrich at the grain boundary (point *G*) rather than react with Al atoms to form intermetallic compounds.

Table 3 EDS analysis results of different points in Figs. 5 and 6

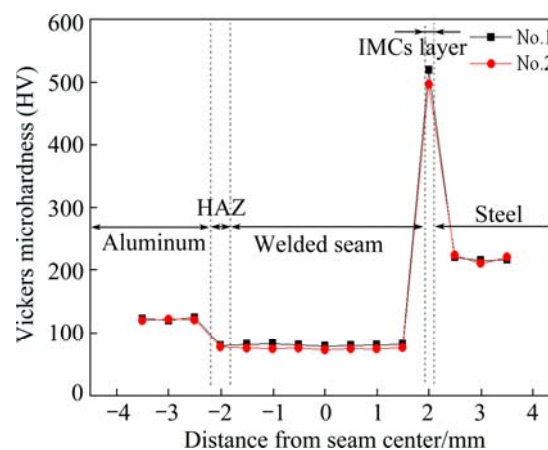
Point	Al		Mg		Zn		Cr		Ni		Fe		Possible phase
	w/%	x/%	w/%	x/%	w/%	x/%	w/%	x/%	w/%	x/%	w/%	x/%	
A	74.26	85.12	0.16	0.77	0.72	0.34	5.90	3.51	0.33	0.18	17.53	9.71	Fe ₂ Al ₅
B	81.63	88.91	1.59	2.04	0.46	0.22	4.87	2.76	0.24	0.13	10.19	5.36	FeAl ₃
C	70.68	82.69	0.25	8.71	–	–	7.55	4.92	2.87	1.66	18.65	10.41	Fe ₂ Al ₅ , (Fe,Cr,Ni)
D	80.12	88.65	1.27	1.50	–	–	6.50	3.58	2.52	1.19	9.59	5.08	FeAl ₃ , (Fe,Cr,Ni)
E	87.69	92.93	1.43	1.71	3.18	1.41	1.69	0.94	0.40	0.20	4.56	2.29	Fe _x Al _y , Mg _x Zn _y
F	96.27	98.02	0.57	0.64	3.12	1.31	–	–	–	–	0.03	0.01	α(Al), (Mg,Zn)
G	84.45	93.05	1.33	1.53	2.90	1.24	2.23	1.19	1.25	0.59	4.85	2.39	α(Al), (Fe,Cr,Ni), (Mg,Zn)
H	94.11	96.33	1.59	1.81	3.78	1.60	0.22	0.12	0.04	0.02	0.27	0.13	α(Al), (Fe,Cr,Ni,Mg,Zn)

**Fig. 6** SEM backscattering images of seam center: (a) Zone D in Fig. 3(a); (b) Zone D in Fig. 3(b)

3.3 Mechanical properties

Vickers micro-hardness of the dissimilar metals butt joint was measured with micro-hardness tester with 10 N loading force for 10 s holding time. The hardness distribution profile is shown in Fig. 7. With regard to both No. 1 joint and No. 2 joint, the hardness values present three footsteps in aluminum alloy, welded seam and steel base metal, respectively, and decreased suddenly in HAZ zone and increased suddenly in IMCs layer. Because the filler metal was pure Al, leading to no many reinforce phases in welded seam, and the hardness of welded seam is lower than that of the tough aluminum base metal. But the hardness of welded seam of No. 1 joint is little higher than that of No. 2 joint, which may be caused by the dispersed intermetallic phases in welded seam of No. 1 joint, as shown in Fig. 6(a). And the hardness of IMCs layer of No. 2 joint is little lower than that of No. 1 joint, because contents of Cr and Ni atoms replacing Fe in IMCs layer of No. 2 joint can reduce its hardness, which can also enhance the properties of IMCs layer [8].

The tensile properties of the welds were also examined by a electronic universal testing machine at room temperature with a loading rate of 1 mm/min. The tensile strengths of two joints are shown in Fig. 8. The tensile strengths of three specimens of No. 2 joint

**Fig. 7** Hardness distribution of butt joint

are obviously higher than those of No. 1 joint. The average tensile strength of No. 2 joint reaches 146.7 MPa, which is higher than 96.7 MPa, the average tensile strength of No. 1 joint.

The macro-fracture profiles of the two butt joints are shown in Fig. 9. The crack of No. 1 joint initiated from the IMCs layer and ran through the whole layer to form the fracture surface, as shown in Fig. 9(a). While the crack of No. 2 joint initiated from the IMCs layer and ran through the whole layer and penetrated into the upper part of welded seam to form the fracture surface, leading

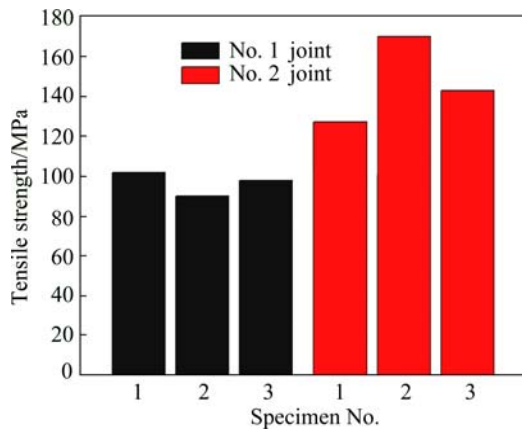


Fig. 8 Tensile strength of butt joint

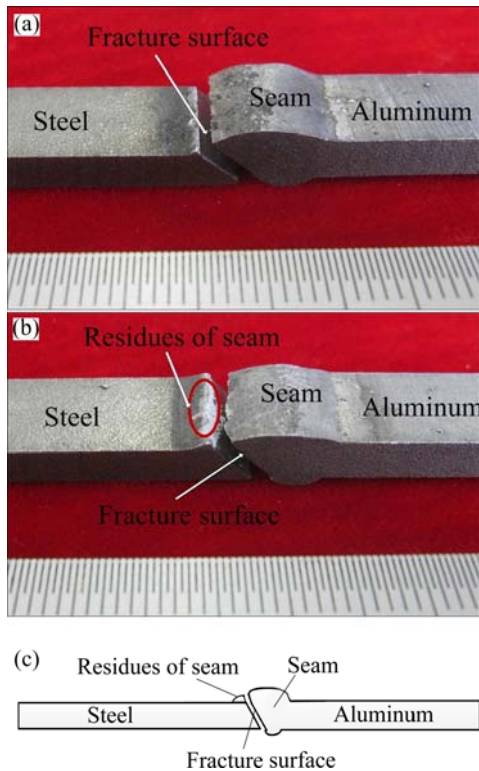


Fig. 9 Macro-fracture profiles of aluminum–steel butt No. 1 joint (a), No. 2 joint (b) and failure mode of No. 2 joint (c)

to residues of seam on the steel surface, as shown in Fig. 9(b) and Fig. 9(c). The ideal wetting ability of molten metal on the upper surface of steel, as shown in Fig. 4(b), changed the fracture path and the enhanced IMCs layer by the Cr and Ni made the tensile strength of No. 2 joint higher than that of No. 1, due to the auxiliary TIG arc.

Figure 10 shows the SEM images of the fracture surface. The fracture surface of No. 1 joint demonstrated a brittle structure, as shown in Fig. 10(b), and there was no formation of Al–Fe compound in the white part. For No. 2 joint, the fracture surface shows a mixed fracture

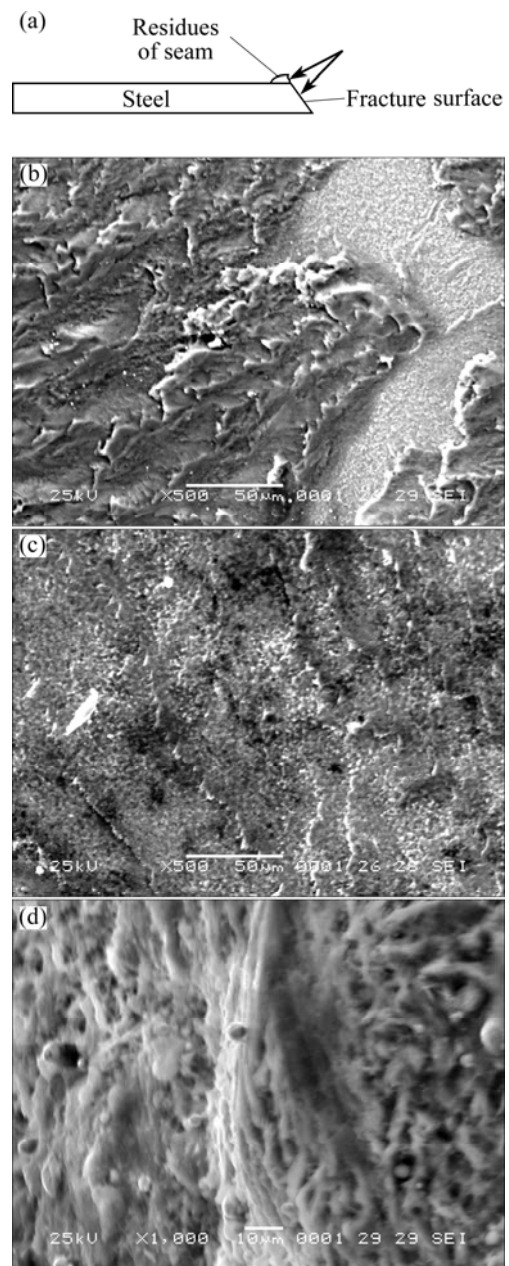


Fig. 10 SEM images of fracture surface: (a) Steel fracture sample of No. 1 joint; (b) On steel side of No. 1 joint; (c) On steel side of No. 2 joint; (d) On residual seam of No. 2 joint

mode of brittle and ductile fracture, as shown in Fig. 10(c). The fracture surface of residual seam exhibited ductile fracture characteristics, as shown in Fig. 10(d). All the above mentioned fracture characteristics proved that the tensile strength of No. 2 joint is higher than that of No. 1 joint.

The X-ray diffraction profiles of the fracture surfaces on steel side as shown in Figs. 10(b) and (c), are shown in Fig. 11. For the No. 1 joint, the fracture occurred at the Fe₂Al₅ layer, and the fracture of No. 2 joint also occurred at the Fe₂Al₅ layer. But (Fe, Cr) and (Cr, Ni) phases also presented on the fracture surface of

No. 2 joint, which proved that the dissolution of Cr and Ni elements was increased by the auxiliary TIG arc and then the property of IMCs layer could be improved. The XRD results of IMCs layer agreed with the possible phases deduced by EDS analysis results in Table 3.

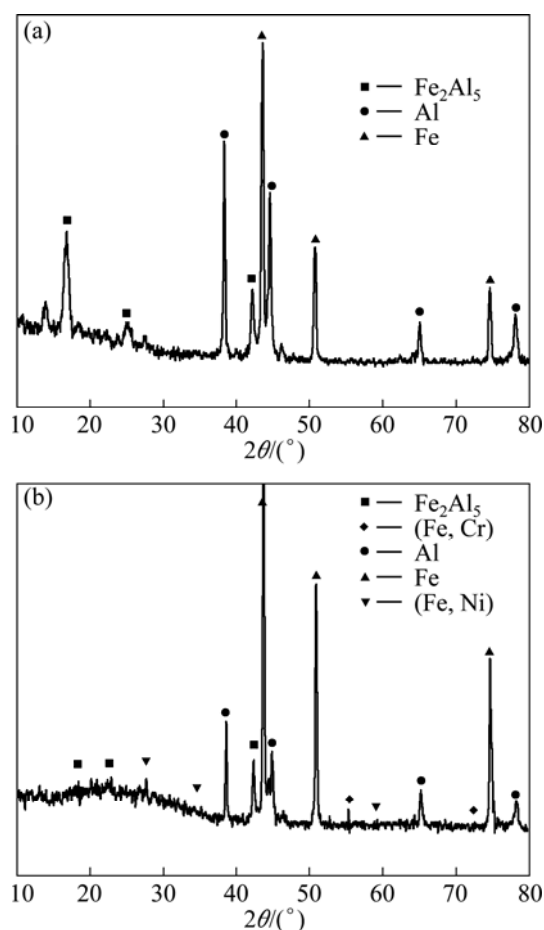


Fig. 11 XRD patterns of fracture surfaces on steel side: (a) No. 1 joint; (b) No. 2 joint

4 Conclusions

1) A new hybrid welding process was successfully constructed to join aluminum alloy to stainless steel butt joint.

2) Additional heat on steel side brought by the auxiliary TIG arc could optimize the wetting performance of molten metal and make it spread more fully on upper surfaces, front and back surfaces of steel to form a sound brazing joint.

3) The IMCs layer mainly consisted of Fe–Al intermetallic compounds and the auxiliary TIG arc could make the IMCs layer homogenize and increase the dissolve of non-iron atoms in the molten metal.

4) The average tensile strength of joint obtained with the auxiliary TIG arc could increase by 51%, compared with the joint made with conventional process.

References

- [1] FRIDLINDER I N, SISTER V G, GRUSHKO O E, BERTENEV V V, SHEVELEVA L M, VANOVA L A. Aluminum alloys: Promising materials in the automotive industry [J]. *Metal Science and Heat Treatment*, 2002, 44: 365–370.
- [2] SHI Y, ZHANG H, TAKEHIRO W, TANG J. CW/PW dual-beam YAG laser welding of steel/aluminum alloy sheets [J]. *Optics and Lasers in Engineering*, 2010, 48: 732–736.
- [3] ALEXANDRE M, RAJASHEKAR S, ALEXIS D, MICHEL S, SIMONE M, DOMINIQUE G, EUGEN C. Dissimilar material joining using laser (aluminum to steel using zinc-based filler wire) [J]. *Optics and Laser Technology*, 2007, 39: 652–661.
- [4] SONG J L, LIN S B, YANG C L, MA G C, LIU H. Spreading behavior and microstructure characteristics of dissimilar metals TIG welding–brazing of aluminum alloy to stainless steel [J]. *Materials Science and Engineering A*, 2009, 509: 31–40.
- [5] UZUN H, DONNE C D, ARGAGNOTTO A, GHIDINI T, GAMBARO C. Friction stir welding of dissimilar Al 6013-T4 To X5CrNi18-10 stainless steel [J]. *Materials & Design*, 2005, 26: 41–46.
- [6] LIU H W, GUO C, CHENG Y, LIU X F, SHAO G J. Interfacial strength and structure of stainless steel–semi-solid aluminum alloy clad metal [J]. *Materials Letters*, 2006, 60: 180–184.
- [7] AIZAWA T, KASHANI M, OKAGAWA K. Application of magnetic pulse welding for aluminum alloys and SPCC steel sheet joints [J]. *Welding Journal*, 2007, 86: 119–124.
- [8] LIN S B, SONG J L, YANG C L, FAN C L, ZHANG D W. Brazability of dissimilar metals tungsten inert gas butt welding–brazing between aluminum alloy and stainless steel with Al–Cu filler metal [J]. *Materials & Design*, 2010, 31: 2637–2642.
- [9] TABAN E, GOULD J E, LIPPOLD J C. Characterization of 6061-T6 aluminum alloy to AISI 1018 steel interfaces during joining and thermo-mechanical conditioning [J]. *Materials Science and Engineering A*, 2010, 527: 1704–1708.
- [10] TRAVESSA D, FERRANTE M, OUDEN G. Diffusion bonding of aluminum oxide to stainless steel using stress relief interlayers [J]. *Materials Science and Engineering A*, 2002, 337: 287–296.
- [11] WATANABE T, TAKAYAMA H, YANAGISAWA A. Joining of aluminum alloy to steel by friction stir welding [J]. *Journal of Materials Processing Technology*, 2006, 178: 342–349.
- [12] NEZHAD M S A, ARDAKANI A H. A study of joint quality of aluminum and low carbon steel strips by warm rolling [J]. *Materials & Design*, 2009, 30: 1103–1109.
- [13] LIU P, LI Y, WANG J, GUO J. Vacuum brazing technology and microstructure near the interface of Al/18-8 stainless steel [J]. *Materials Research Bulletin*, 2003, 38: 1493–1499.
- [14] QIU R, ZHANG K, TU Y, SHI H, IWAMOTO C, SATONAKA S. Interfacial characterization of joint between mild steel and aluminum alloy welded by resistance spot welding [J]. *Materials Characterization*, 2010, 61: 684–688.
- [15] DONG Hong-gang, HU Wen-jin, DUAN Yu-ping, WANG Xu-dong, DONG Chuang. Dissimilar metal joining of aluminum alloy to galvanized steel with Al–Si, Al–Cu, Al–Si–Cu and Zn–Al filler wires [J]. *Journal of Materials Processing Technology*, 2012, 212: 458–464.
- [16] SONG Jian-ling, LIN San-bao, YANG Chun-li, MA Guang-chao. Characteristics of pre-coating TIG welding–brazing joint of aluminum alloy to stainless steel [J]. *The Chinese Journal of Nonferrous Metals*, 2009, 19(7): 1209–1215. (in Chinese)
- [17] ZHANG Hong-tao, LIU Jia-kun. Microstructure characteristics and mechanical property of aluminum alloy/stainless steel lap joints

- fabricated by MIG welding–brazing process [J]. *Materials Science and Engineering A*, 2011, 528: 6179–6185.
- [18] SIERRA G, PEYRE P, DESCHAUX-BEAUME F, STUART D, FRAS G. Steel to aluminium braze welding by laser process with Al–12Si filler wire [J]. *Science and Technology of Welding and Joining*, 2008, 13: 430–437.
- [19] ROULIN M, LUSTER J W, KARADENZ G, MORTENSEN A. Strength and structure of furnace-brazed joints between aluminum and stainless steel [J]. *Welding Journal*, 1999, 78(5): s151–s155.
- [20] KATTNER U R. Binary alloy phase diagrams [M]. Materials Park, OH: ASM International, 1990: 147.
- [21] SONG J L, LIN S B, YANG C L, FAN C L. Effects of Si additions on intermetallic compound layer of aluminum–steel TIG welding–brazing joint [J]. *Journal of Alloys and Compounds*, 2009, 488: 217–222.
- [22] DONG Hong-gang, YANG Li-qun, ZHAI Nan, DONG Chuang. Analysis on microstructure and mechanical properties of aluminum alloy/stainless steel joint made with flux-cored filler metal [J]. *Transaction of the China Welding Institution*, 2011, 32(10): 1–4. (in Chinese)
- [23] QIU R, IWAMOTO C, SATONAKA S. Interfacial microstructure and strength of steel/aluminum alloy joints welded by resistance spot welding with cover plate [J]. *Journal of Materials Processing Technology*, 2009, 209(8): 4186–4193.

辅助 TIG 电弧对铝合金/不锈钢 MIG 熔–钎焊接头形成机制及显微组织的影响

张洪涛, 刘积厚, 冯吉才

哈尔滨工业大学(威海) 材料科学与工程学院, 山东省特种焊接技术重点实验室, 威海 264209

摘要: 利用一种新型的复合熔–钎焊工艺焊接铝合金和不锈钢。在 MIG 熔–钎焊工艺中, 因钢的导热性差而导致焊缝钢侧的温度梯度变化剧烈, 利用 TIG 电弧加热钢侧可改善这一现象。TIG 辅助电弧改善了熔融金属在钢基体上的润湿性, 使熔融金属能充分地在钢侧焊接坡口区正面及背面充分润湿, 所得接头成形良好; 增加了金属间化合物层内 Cr、Ni 的含量, 提高了其力学性能; 同时, 改变了化合物层的形貌, 增强了其与焊缝的结合强度。TIG 辅助焊接工艺下获得接头的平均拉伸强度(146.7 MPa)明显高于无辅助 TIG 电弧下接头的拉伸强度(96.7 MPa)。
关键词: 熔–钎焊; 辅助 TIG 电弧; 润湿性; 金属间化合物层; 力学性能

(Edited by Xiang-qun LI)